Magma mixing and high fountaining during the 1959 Kīlauea Iki eruption, Hawai`i

I. Sides[1], M. Edmonds[1*], J. Maclennan[1], B. Houghton[2], D. Swanson[3], M. Steele-Macinnis[4]

1 Earth Sciences Department, University of Cambridge, United Kingdom

2 Department of Geology and Geophysics, University of Hawai`i, Honolulu, Hawai`i, USA

3 Hawaiian Volcano Observatory, US Geological Survey, Hawai`i National Park, HI 96718, USA

4 Institute for Geochemistry and PetrologyETH Zurich, Clausiusstrasse 25, NWCH 8092 Zurich, Switzerland

* Corresponding author

Abstract

The 1959 Kīlauea Iki eruption provides a unique opportunity to investigate the process of shallow magma mixing, its impact on the magmatic volatile budget and its role in triggering and driving episodes of Hawaiian fountaining. Melt inclusions hosted by olivine record a continuous decrease in H_2O concentration through the 17 episodes of the eruption, while CO_2 concentrations correlate with the degree of post-entrapment crystallization of olivine on the inclusion walls. Geochemical data, when combined with the magma budget and with contemporaneous eruption observations, show complex mixing between episodes involving hot, geochemically heterogeneous melts from depth, likely carrying exsolved vapour, and melts which had erupted at the surface, degassed and drained-back into the vent. The drained-back melts acted as a coolant, inducing rapid cooling of the more primitive melts and their olivines at shallow depths and inducing crystallization and vesiculation and triggering renewed fountaining. A consequence of the mixing is that the melts became vapor-undersaturated, so equilibration pressures cannot be inferred from them using saturation models. After the melt inclusions were trapped, continued growth of vapor bubbles, caused by enhanced post-entrapment crystallization, sequestered a large fraction of CO_2 from the melt within the inclusions. This study, while cautioning against accepting melt inclusion CO_2 concentrations "as measured" in mixed magmas, also illustrates that careful analysis and interpretation of post-entrapment modifications can turn this apparent challenge into a way to yield novel useful insights into the geochemical controls on eruption intensity.

Keywords: Hawaiian Fountaining; Mixing; Volatiles; Degassing; Melt Inclusions; Kīlauea

6199 words

1. Introduction

The 1959 eruption of Kīlauea Iki, Hawai`i (**figure 1**), was remarkable for its close-spaced, episodic high fountains (Richter et al., 1970), the highly magnesian magmas erupted (Murata and Richter, 1966; Wright, 1973; Helz, 1987; Anderson and Brown, 1992), the repetitive and voluminous draining of erupted lavas back into the vent between episodes (Eaton et al., 1987; Wallace and Anderson, 1998) and the detailed set of observations of fountain height, lava lake level, repose period durations and contemporaneous ground deformation and seismicity (Macdonald, 1962; Richter et al., 1970; Eaton et al., 1987; **Table 1**). The tephra products of most individual episodes have been identified and characterized (Klawonn et al., 2014; Stovall et al., 2012; Stovall et al., 2011). This eruption then, lends itself well to a study aiming to understand how high fountaining is triggered and sustained and to analyze the role of magma mixing in influencing eruption dynamics. Mixing involved hot primitive melts supplied from depth into the shallow magma reservoir beneath the summit of Kīlauea (at a depth of 2-5 km; (Fiske and Kinoshita, 1969; Pietruszka and Garcia, 1999b; Ryan et al., 1981), stored melts in the magma reservoir, and cooler, degassed melts that drained-back into the conduit after each of 16 high fountaining episodes of the eruption.

fountaining episodes of the eruption.

Understanding Hawaiian fountaining has been the focus of intensive study over the past 30 years. Two conceptual end member models were proposed in the 1980s that differ in their treatment of the flow dynamics. The first proposed that eruption style is dependent on the ascent rate of the magmas (Fagents and Wilson, 1995; Head and Wilson, 1987; Parfitt, 2004; Slezin, 2003; Wilson and Head, 1988). Rising magma exolves gas into existing and nucleating bubbles, which may become buoyant relative to the melt. If the ascent rate of the magma is sufficiently fast, the bubbles are coupled with the magma (homogeneous two-phase flow), eventually leading to fragmentation and lava fountaining. A feature of this model is that fountain heights are theoretically related to pre-eruptive melt H_2O content (Head and Wilson, 1987; Parfitt et al., 1995). An alternative model proposed that fountains originate from complete collapse of a foam layer, formed by accumulation of bubbles at the roof of a magma reservoir (Jaupart and Vergniolle, 1988; Vergniolle, 2008; Vergniolle and Jaupart, 1986). At a critical thickness, the foam undergoes complete, near-instantaneous collapse, leading to separated two-phase flow in the conduit and a sustained high fountain until the foam layer and gas supply is depleted (Vergniolle and Jaupart, 1986). In contrast to the previous model, where the fountain-driving gas is H_2O (Head and Wilson, 1987; Parfitt, 2004), the foam-accumulation model requires that CO_2 drives the fountain, because at magma reservoir depths H_2O largely remains in solution (Dixon et al., 1991; Gerlach and Graeber, 1985). The foam accumulation model was applied to Kīlauea Iki by Vergniolle (2008), who used the repose times and eruption rates during each episode to estimate a rate of gas fluxing and bubble accumulation during the eruption. More recent work on fountaining suggests that these two models may be end members, with a full continuum of intermediate two phase flow behaviors lying in between (Houghton and Gonnermann, 2008; James et al., 2013). The challenges involved in understanding how fountains work during historical eruptions stem largely from the difficulty in quantifying the amount and flux of exsolved vapour that co-existed with magma, for which there exists no petrological record. These volatiles were undoubtedly of singular importance for triggering and driving fountaining, yet we only have available information about the pre-eruptive abundance of dissolved volatiles in melt inclusions, which themselves have been subject to post-entrapment processes, to unravel degassing mechanisms.

A magma budget for the 1959 eruption was established from geophysical observations of deformation and eruption and drained-back lava volume estimates (Richter et al., 1970; (Eaton et al., 1987); **Table 1**). Around 30 x 10^6 m^3 of lava was erupted during episode 1 and was, over the course of the eruption, more than replaced by 60 x 10^6 m^3 of picritic magma intruding the reservoir from depth, mainly during episodes 1 to 7 (**Figure 2**). In all, 63 x 10^6 m^3 lava drained back into the vent, and drained-back lavas were re-erupted over and over, such that the volume of the lava lake before and after each episode remained approximately constant during episodes 7 to 17. During the later episodes then, when very little magma was being supplied from depth and drained-back lava dominated the magma budget, it is unclear what the "driving force" for repeated eruptions was. Eaton et al. (1987) speculated that CO_2 might be the driving gas for a "vesiculation pump", driving the fountains by lowering the density and therefore pressure of the magma column in the conduit and further, that fountain height might be determined by the amount and composition of accumulated gases, an idea that has never been tested.

A consequence of the magma budget produced by Eaton et al. (1987) is that magma mixing was a significant process both in the shallow magma reservoir and in the conduit prior to and during episodes of fountaining. Recent studies of the trace element geochemistry of melt inclusions and of whole rocks have shown that magmas supplied to Kīlauea's deep plumbing system are heterogeneous in terms of their isotopic and trace element ratios, indicating coupled changes in mantle source composition and the degree of partial melting over 10^2-10^3 year timescales at Kīlauea (Edmonds et al., 2014; Garcia et al., 2003; Marske et al., 2010; Pietruszka and Garcia, 1999a; Pietruszka et al., 2012; Sides et al., 2014). The 1959 Kīlauea Iki eruption occurred during a period spanning the mid-20^{th} century that was characterized by short-lived, explosive eruptions that were fed by magmas that were statistically more primitive and geochemically enriched in LREE and volatiles (Sides et al., 2014). A shallow magma reservoir beneath the summit allows homogenization of heterogeneous melts during prolonged storage. Mixing between deep, stored and drained-back melts should then be "trackable" via melt inclusion geochemistry. It has been

LREE and volatiles (Sides et al., 2014). A shallow magma reservoir beneath the summit allows homogenization of heterogeneous melts during prolonged storage. Mixing between deep, stored and drained-back melts should then be "trackable" via melt inclusion geochemistry. It has been proposed previously that the Kīlauea Iki eruption involved the mixing of two end member magmas: S1 (intruded) and S2 (stored) (Murata and Richter, 1966; Wright, 1973); we extend this model in the current work by considering the detailed trace element geochemistry of olivine-hosted melt inclusions. This paper aims, therefore, to elucidate mechanisms triggering and driving fountains, as well as the role of magma mixing in influencing eruption dynamics during the 1959 eruption of Kīlauea Iki using the major, trace and volatile element geochemistry of olivine-hosted melt inclusions from 10 well constrained episodes of the eruption.

2. Methods

2.1. *Sampling*

Tephra samples from 10 episodes were collected from stratigraphy exposed in three pits (KI-07-14, KI-06-16 and KI-06-13; (Stovall et al., 2012); **Figure 1b**) downwind of the eruption vent. Episode 1 tephra is dominated by glassy achnelith lapilli including Pele's tears, small glass spheres, shards and rods and fluidal clasts with shiny external surfaces displaying flow lines and vesicular interiors with mm- to cm-sized bubbles. Deposits produced by the highest fountains (episodes 3, 15 and 16) are characterized by a larger mean grain size of several cm, with spatter bombs up to 25 cm in length together with ragged, highly vesicular, golden to light brown pumice. Detailed textural and density analyses of clasts for episodes 1, 15 and 16 are presented by Stovall et al. (2011, 2012). Crystal contents are generally < 10 vol%. Tephra from the 1960 flank eruption at Kapoho was also sampled from a section of the 'pumice loaf' described by Richter (1970) that formed during vigorous fountaining formed on January 27, 1960.

2.2. *Microanalysis*

Samples of cm-sized lapilli were dried and crushed and olivines picked and mounted in epoxy resin. Care was taken to analyze melt inclusions hosted by olivine with a range of morphologies and to avoid over-sampling inclusions from the largest grains with obvious resorption textures. Olivine-hosted melt inclusions were exposed by grinding and polishing. Matrix glasses, olivines and their melt inclusions were analyzed for major, volatile and trace element compositions using electron probe, secondary ion mass spectrometry (SIMS) and laser ablation inductively-coupled mass spectrometry (LA-ICP-MS) respectively (see **supplementary material** for analytical methods). All melt inclusion compositions were compared to the composition of the olivine host adjacent to the melt inclusion and were found to have undergone variable amounts of post-entrapment crystallization (PEC), up to 28% (Danyushevsky and Plechov, 2011) (methods described in **supplementary material**). All of the inclusions analyzed were naturally quenched, >35 μm in size and not necked or breached by cracks.

3. Results

3.1. *Petrography and olivine chemistry*

The Kīlauea Iki samples are olivine-phyric, with ubiquitous 0.5–5.0 mm unaltered olivines. Clinopyroxene and plagioclase are rare or absent. Olivines occur as subhedral phenocrysts and as aggregates, including all of the morphology groups identified by Helz (1987), recently interpreted as the products of rapid crystallization (Welsch et al., 2013). The olivines contain brown glass inclusions up to 300 μm in diameter. Of the 116 melt inclusions analyzed, 48 contained a vapour bubble that survived inclusion exposure and polishing, typically occupying <7 vol% of the inclusion. Forsterite contents of the phenocryst cores range from 78.9 to 88.6 mol% Fo. The olivine populations for each episode show a broad range of Fo content which does not correlate with the average matrix glass compositions (**Figure 3**), with all olivine compositions lying above the line of K_D=0.3, where K_D is equal to $K_D = \left(X_{Fe^{2+}} / X_{Mg}\right)_{ol} \Big/ \left(X_{Fe^{2+}} / X_{Mg}\right)_{liq}$, where X are molar fractions of Fe^{2+} and Mg in the olivine and in the melt (liq) (Roeder and Emslie, 1970), indicating that the olivine cores were not in equilibrium with their carrier melts at the time of eruption. Some of the

the line of K_D=0.3, where K_D is equal to [illegible], where X are molar fractions of Fe^{2+} and Mg in the olivine and in the melt (liq) (Roeder and Emslie, 1970), indicating that the olivine cores were not in equilibrium with their carrier melts at the time of eruption. Some of the olivines erupted during episode 1 had a more primitive, Fo-rich composition than those of the later episodes (**figure 3**).

3.2. Major and trace element geochemistry

The melt inclusion compositions, when corrected for PEC, range from 7.2 to 13.9 wt% MgO, compared with the significantly more evolved compositions of the matrix glasses at 6.3–10.3 wt% MgO. The trends are controlled by olivine fractionation. The whole rock data show the effect of olivine accumulation, with lavas containing up to nearly 20 wt% MgO (Murata and Richter, 1966). A decrease in CaO/Al_2O_3 ratios of the glasses at lower MgO concentrations suggests some late clinopyroxene fractionation. There is considerable scatter in the concentrations of minor element oxides e.g. P_2O_5, TiO_2 and K_2O at a given MgO value outside the analytical error (**figure 4**), deviating from the olivine-dominated liquid line of descent defined by the whole rock and glass compositions.

Trace element abundances are consistent with the fractionation trends discussed above. Decreasing MgO is accompanied by increases in highly incompatible elements between the melt inclusion and glass compositions (**figure 4**). Scandium abundance is consistent with a degree of clinopyroxene fractionation (**figure 4**). The melt inclusions display a much greater variation in the trace element contents for a fixed MgO content than do the matrix glasses that is outside analytical error. There is a large degree of trace element variation within the inclusion populations from each individual episode, with no clear temporal trends (**figure 5a**). The matrix glasses define almost linear trends in La–Y and Nb–Y space; however the melt inclusion compositions are more variable and span a broad range of ratios; there are no clear temporal variations (**figure 5a**). The degree of variability of trace element ratios in melt inclusions (e.g. La/Yb, Nb/Y), expressed as their standard deviation, correlates with the amount of inflation recorded prior to each eruption episode (**figure 5b**).

3.3. Volatile geochemistry

Water (H_2O) and carbon dioxide (CO_2) concentrations in the melt inclusions range from 0.09 to 0.64 wt% and from 31 to 656 ppm respectively (**figure 6a, b**), within the range observed previously (Anderson and Brown, 1993; Wallace and Anderson, 1998). Matrix glass compositions vary between 0.04 and 0.11 wt% H_2O, and CO_2 concentrations are below detection limits. The pressures obtained from melt-vapor equilibria (Dixon, 1997; Newman and Lowenstern, 2002) are <150 MPa. However, the melts may be undersaturated with respect to H_2O if they are the product of mixing between saturated and undersaturated melts (see later). Just as importantly, **figure 6a** shows that there is a clear relationship between the CO_2 concentration recorded in a melt inclusion and the degree of PEC. The inclusions that have undergone the highest degree of cooling post-entrapment, and hence the most crystallization of olivine onto the walls of the inclusion, have the lowest concentration of CO_2. This is caused by the sequestration of CO_2 into vapor bubbles, promoted by PEC (Steele-Macinnis et al., 2011), discussed more later. A striking feature of **figure 6b, c, d** is the temporal trend in H_2O concentrations from episode to episode. Episode 1 has the largest range in and the highest H_2O values. Melt inclusions erupted during episodes 15 and 16 are the most H_2O-poor, with most concentrations grouping at significantly lower H_2O and CO_2 values than those of earlier episodes.

Sulfur (S) concentrations range from 175 to 1530 ppm in the melt inclusions and from 35 to 171 ppm in the matrix glasses (**figure 6c**), consistent with extensive, but incomplete, syn-eruptive degassing. S does not correlate with non-volatile incompatible trace elements, indicating that processes other than fractionation are exerting a dominant control over melt concentrations. Chlorine and fluorine (not shown) concentrations in the inclusions range from 90 to 410 ppm and 180 to 810 ppm respectively (**figure 6d**). Halogens are more soluble than other volatile species (Sigvaldason and Óskarsson, 1976); (Edmonds et al., 2009), but neither element correlates with non-volatile incompatible elements (not shown). Chlorine concentrations are elevated in episode 3 melt inclusions relative to the other episodes. Matrix glasses contain 111-268 ppm Cl and 541–714 ppm F. There is no clear relationship between either of these elements and other volatile elements such as H_2O (**figure 6d**).

714 ppm F. There is no clear relationship between either of these elements and other volatile elements such as H_2O (**figure 6d**).

When compared with measures of eruption dynamics such as fountain height, it can be seen that in general the highest fountains erupt tephra containing melt inclusions with the lowest CO_2 concentrations (**figure 7**). While there is considerable scatter within individual episodes, the mean CO_2 concentration in melt inclusions erupted during each episode correlates negatively with the maximum and mean fountain heights, with r values (correlation coefficients) of -0.77 and -0.73 respectively (**figure 7b**).

4. Discussion

4.1. Provenance of the melt inclusions and their relationship with the carrier liquids

In order to use the melt inclusion compositions for constraining pre- and syn-eruptive processes, it is necessary to consider whether the olivine-hosted inclusions are genetically related to their host-carrier melts. The poor correlation between the core olivine composition and the matrix glass compositions (**figure 3**) implies disequilibrium. Disequilibrium may be induced if crystallization occurred prior to extensive magma mixing within the summit reservoir, or if the high-Fo olivines were xenocrysts formed in the mantle or cumulates from previous magmatic events. The latter explanation is discounted owing to the moderate CaO contents of the crystals (0.25– 0.35 wt%; (Garcia et al., 2003; Jurewicz and Watson, 1988). The olivines may be antecrysts, crystals that formed in the plumbing system of the eruption but were not in chemical equilibrium with the carrier melts, which were products of mixing with more evolved, stored melts, at the time of eruption (Davidson et al., 2007; Maclennan, 2008).

The melt inclusions show considerably larger degrees of compositional heterogeneity in terms of trace element ratios than the matrix glasses (**figure 5a**). These ratios, such as La/Yb, are not affected by fractional crystallization (the fractionating assemblage is olivine-only; **figure 4**) or by post-entrapment crystallization, and therefore reflect compositional differences inherited from primary melts. This greater degree of compositional variability in melt inclusions has been widely observed and discussed, and is thought to be related to the mixing process, whereby heterogeneous melts produced in the mantle are gradually mixed together, eventually producing relatively homogeneous carrier liquids in the shallow plumbing system (Kent and Elliott, 2002; Kent, 2008; Sobolev, 1996). The composition of the matrix glasses lies within the ranges defined by the melt inclusions, consistent with their being genetically related by mixing (**figure 5a**).

4.2. Constraints on magma mixing and fractionation from major and trace elements

Mixing and fractionation of the Kīlauea Iki magmas has been investigated previously using whole rock compositions (Murata and Richter, 1966; Wright, 1973; Helz, 1987). Melt inclusion compositions are unaffected by olivine accumulation and are more sensitive to melt mixing processes. The MgO content of the most primitive melt inclusions (after correction for PEC) is comparable with the highest MgO concentrations measured for Kīlauea in submarine glasses from the east rift zone (15 wt%) (Clague et al., 1991) and may be close to primary. Though olivine fractionation trends between the glasses and inclusions are present, the heterogeneity in minor and trace element compositions (**figures 4, 5**) likely reflects primary melt compositional variability propagated during olivine crystallization. It is possible that some of the variability observed in slow-diffusing species (in silicate melts) such as phosphorus is a result of rapid crystal growth and diffusive "pile-up" (Baker, 2008), but this does not explain the majority of the data.

Two compositionally distinct end members from episode 1 were recognized from whole rock major element studies (S1 and S2; Murata and Richter, 1966; Wright, 1973; marked on **figure 4**). S1 is a CaO-rich composition and S2 lies at the more evolved, Mg-poor end of the compositional range. It was proposed that the hotter, more MgO-rich S1 ascended from mantle depths during the August earthquake swarms, arrived at the base of the summit reservoir by late September 1959 and encountered a separate body of older, stored S2 magma (Wright, 1973; Helz, 1987). Whole rock data are explained well by such a mixing model. It is clear, however, that the matrix glass and melt inclusion populations show variability outside the range for mixing of S1 and S2 components. The mixing model proposed by Murata and Richter (1966) involves only pre-eruptive mixing between two compositions, yet the volume data (Eaton et al., 1987; **Table 1;**

glass and melt inclusion populations show variability outside the range for mixing of S1 and S2 components. The mixing model proposed by Murata and Richter (1966) involves only pre-eruptive mixing between two compositions, yet the volume data (Eaton et al., 1987; **Table 1; figure 2**) demonstrates that magma reservoir volume was constantly changing throughout the eruption due to both the continued arrival of new melt input from depth and the drain-back of erupted lavas. It is likely that the interaction of drained-back melts with new input from depth produced the non-equilibrium conditions necessary for rapid olivine growth and melt inclusion entrapment. We propose that the inclusions record incomplete mixing between heterogeneous melts from depth, and more homogeneous stored and drained-back melts. The incompleteness of mixing is supported by the positive correlation between the volume of reservoir inflation (**Table 1**) and the standard deviation of melt inclusion Nb/Y for each episode (**figure 5b**; which, when fitted by a logarithmic regression, has an r^2 value of of 0.84). We interpret this relationship to show that the intruding magma has a higher degree of geochemical heterogeneity, so when intruding melt volumes are large compared to stored volumes, a greater degree of heterogeneity is displayed by the mixed melt. Melt was trapped as inclusions before mixing could homogenize the mixed melt composition. Repeated replenishment and drain-back, with the accompanying turbulence, may have been a very effective means of homogenizing the contents of the reservoir (Eaton et al., 1987) and may explain the limited glass heterogeneity in the host glass compositions. The relationship in **figure 5b** also illustrates, in accordance with the magma budget deduced by Eaton et al. (1987) that the volume of intruding magma is roughly equal to the volume of the reservoir. Whether this volume (40-50 million m^3) is the total volume of the magma reservoir, or that of an "active" sub-volume, is unclear.

4.3. Drain-back and magma mixing controls H_2O abundance in melt inclusions

Dissolved H_2O concentrations of the melt inclusions decrease continuously throughout the eruption (**figure 6b**). The trend in H_2O concentrations is similar to that observed in the four episodes analyzed by Wallace and Anderson (1998), which they attributed to increasing degrees of mixing between drained-back lavas with undegassed magma in the shallow reservoir. We explore the range of possible explanations for the trends in volatile species: (1) the loss of H_2O from the inclusions by post-entrapment diffusive re-equilibration with external melt; (2) "flushing" of the melt by a decoupled CO_2-rich gas phase when the incoming melts are known to exist with at least 0.6 wt% exsolved vapour; from volcanic gas fluxes (Gerlach et al., 2002); (3) mixing between drained-back and primitive gas-rich magmas at depth as proposed by Wallace and Anderson (1998) and (4) the effects of post-entrapment crystallization and vapor bubble growth on sequestering CO_2. We discuss each of these below.

Recent studies have shown that olivine-hosted inclusions are susceptible to H_2O-loss or gain by exchange with the external melt via H^+ diffusion through the host-olivine structure (Gaetani et al., 2012; Hauri, 2002). Diffusion would have been possible on the timescales of the Kīlauea Iki eruption, as experimental studies reveal that the process is rapid and can occur in a matter of hours if there is a concentration gradient between the external and trapped melt (Gaetani et al., 2012; Portnyagin et al., 2008). It might be envisaged, for example, that vapor-saturated magma ascended to shallow depths, to perhaps a subsidiary reservoir beneath Kīlauea Iki, at perhaps less than a few hundred metres depth, whereupon the carrier liquid rapidly degassed H_2O and became relatively dry. During residence in this region, H_2O would have diffused out of the melt inclusions and through the olivine host to equilibrate with the carrier liquid. If equilibration proceeded to completion, all melt inclusions would have ended up with the same H_2O content as the carrier liquid. If the process is time-limited, then only partial equilibration would have been achieved. We model this process to assess whether the timescales of the Kīlauea Iki eruption would allow the temporal trend in H_2O observed in the melt inclusions to be generated. Using a diffusion model (Qin et al., 1992) with vacancy-limited proton diffusivity parallel to [001] (Demouchy and Mackwell, 2003) and assuming variable distances of 50 to 400 microns between the inclusion wall and the carrier liquid, we have calculated the H_2O remaining with time in a melt inclusion of 100 microns size, initially containing 1 wt% H_2O, during residence in a carrier liquid containing no H_2O. We find that over the range of realistic inclusion and olivine sizes and temperatures, a model whereby magma is transported to low pressures and held in a subsidiary reservoir prior to eruption will result in extremely rapid equilibration, after only 24-48 hours; it could certainly not be sustained under these conditions for over a month. If such a model was relevant, then melts erupting later than episode 1 should have a fixed melt H_2O content the magnitude of which is dependent on the pressure at which the magma was stored prior to

could certainly not be sustained under these conditions for over a month. If such a model was relevant, then melts erupting later than episode 1 should have a fixed melt H_2O content the magnitude of which is dependent on the pressure at which the magma was stored prior to eruption, which is not observed (**figure 6b**). The second possibility related to diffusion is that the magma reservoir shallowed with time, allowing the steady decrease in melt inclusion H_2O content. We consider this possibility unlikely and it is not supported by the geodetic data (Eaton et al., 1987). We conclude that diffusive loss of hydrogen from the melt inclusions is not a primary control on the temporal trend in melt H_2O, but we do not rule out that it is a secondary process; indeed it would seem that some H_2O loss is almost inevitable given the rapidity of proton diffusion, in agreement with other workers (Lloyd et al., 2013).

Another possible explanation for the continuous decline in H_2O concentrations with time is that the melts were "flushed" by a decoupled CO_2-rich gas from depth that acted to dehydrate the melt by lowering the solubility of H_2O. This mechanism has been proposed to explain the scatter of data away from a closed-path mixing trend on a H_2O-CO_2 plot for basaltic volcanoes such as Etna, Italy (Spilliaert et al., 2006) and Jorullo, Mexico (Johnson et al., 2008), among others. This mechanism would be consistent with previous work on CO_2 abundance at Kīlauea which suggests that primary melts contain 0.3 to 1.0 wt% CO_2, based on volcanic gas fluxes from the summit (Gerlach et al., 2002) and based on an estimate of initial CO_2/Nb concentrations in melt inclusions (Sides et al., 2014). The melt inclusions contain < 800 ppm CO_2, which means that the bulk of the CO_2 in the system must exist as a separate vapor phase in the intruding magmas. Bubble-melt separation occurs at shallow levels of the Kīlauea plumbing system, as evidenced by the persistent plume of CO_2 gas at the summit (Gerlach et al., 2002) and by theoretical models (Bottinga and Javoy, 1991; Vergniolle, 1996), making gas flushing a plausible process in the shallow magma reservoir, which would inevitably cause melt dehydration (Métrich and Wallace, 2008; Moore et al., 1998; Newman and Lowenstern, 2002). There are no data available to indicate whether there was a persistent degassing between fountaining episodes that might support the idea that a large flux of CO_2-rich gas was passing continuously through the magma, but this is very likely, based on typical styles of degassing (Gerlach et al., 2002).

There is no evidence for crystallization of the carrier liquid accompanying gas flushing and melt dehydration due to the increase in solidus temperature, as has been observed in other systems (e.g. up to 14 mol% olivine crystallization at Jorullo, Mexico; Johnson et al., 2008). For a H_2O-poor melt undergoing dehydration, the undercooling is likely to be much less: the removal of 0.5 wt% H_2O will increase the solidus temperature by only around 30-40 °C at 1500 bars, resulting in 3-5 mol% olivine crystallization (from MELTS; Ghiorso and Sack, 1995). If gas flushing and magma dehydration were occurring, we would expect a negative correlation between H_2O and incompatible elements (which should give rise to increases in incompatible element concentrations outside the error), which is not observed. Gas flushing and dehydration would be expected to buffer the CO_2 concentrations in the melt to an approximately constant value if the process is pervasive and efficient (owing to the horizontal isobars on a CO_2-H_2O plot; **figure 6b**), however, the CO_2 concentrations have been overprinted largely by sequestration of CO_2 vapour into a vapor bubble, shown in **figure 6a** and discussed in more detail below. Exsolved vapour must be abundant in the intruding magmas (from volcanic gas fluxes; Gerlach et al., 2002) and almost certainly played an important role in buoyant rise and in driving the fountaining, as proposed by Vergniolle (2008).

The effects of lava drain-back and mixing on melt volatile concentrations may be explored by adaptation and extension of the Wallace and Anderson (1998) model (described in detail in **supplementary material)**. The model is an iterative mass balance calculation, based on the magma volume estimates of Eaton et al. (1987; **Table 1; Figure 2**). **Figure 8** demonstrates a good agreement between the predicted H_2O trends and those observed in the melt inclusions, with an r value of 0.92 describing the correlation between the model and the mean H_2O concentrations for each episode. Throughout the eruption, the volume of new melt supplied from depth decreased more or less continuously (**figure 2**), such that increased cumulative drain-back with little or no new input in later episodes resulted in a decrease in melt H_2O concentrations (such that the pre-eruptive melts became undersaturated with respect to H_2O), consistent with previous

decreased more or less continuously (**figure 2**), such that increased cumulative drain-back with little or no new input in later episodes resulted in a decrease in melt H_2O concentrations (such that the pre-eruptive melts became undersaturated with respect to H_2O), consistent with previous work (Wallace and Anderson, 1998). Measured CO_2 concentrations, however, bear no resemblance to those predicted by the mixing model, with measured values at higher concentrations than predicted, particularly for episodes 6-10 (**figure 8**); this is consistent with evidence that suggests that the CO_2 signature is entirely overprinted by post-entrapment sequestration into a vapor bubble (**figure 6a**).

The concentrations of sulfur and chlorine do not provide additional discriminatory power. **Figure 6c** shows a relationship between H_2O and S for episodes 15 and 16 consistent with low pressure degassing (Gerlach, 1986). Loss of S at constant H_2O concentration is consistent with saturation with a sulphide phase (Wallace and Carmichael, 1992), which may be removed efficiently into a cumulate pile and the concentration of sulfur in the melts may therefore be buffered by a sulfide phase. Chlorine (Cl) and fluorine (F) have a much greater solubility in basaltic melts than H_2O, CO_2 or S and there is considerable overlap between the dissolved concentrations in the residual glasses and the melt inclusions, consistent with halogens exsolving into vapour from Kīlauea melts at pressures <1 MPa (Edmonds et al., 2009; Mather et al., 2012; Sigvaldason and Óskarsson, 1976). The low pressure of exsolution of the halogens, however, means that often their abundance is controlled kinetically, rather than via equilibrium processes, making their interpretation problematic (Edmonds et al., 2009; Mather et al., 2012; Edmonds et al., 2013). The concentrations of sulfur and chlorine are consistent with a magma mixing model, as described above.

In summary, there are a range of processes which might explain the trends shown in **figure 6**, but we propose that the dominant process is magma mixing, which is supported by both the trace and volatile element data (**figures 5, 6**). Magma mixing can explain simultaneously both the trend observed in H_2O concentrations (mixing between degassed and undegassed melts) and also the trends observed in CO_2 concentrations, caused by cooling, post-entrapment crystallization and CO_2 sequestration into a vapour bubble (explained in more detail below). The negative correlation between fountain heights and CO_2 concentrations, showing that the highest fountains are produced when there is the highest degree of post-entrapment cooling of the melt inclusions, further suggests that the mixing process has some control on eruption dynamics. We lay out below our proposed model below to explain how magma mixing might trigger and drive fountaining.

4.4. Magma mixing, rapid vesiculation and fountain triggering

Hot, primitive magmas from depth mixed with cooler, degassed, drained-back lavas after each episode (**figure 9**). As hot magma carrying primitive olivines rose and was juxtaposed with the cooler drained-back and stored reservoir magma, rapid crystallization occurred in the cooling primitive melt at its boundary with the reservoir magma (**figure 9**). Rapid crystallization may explain the crystal growth forms observed in the Kīlauea Iki olivines (Helz, 1987), perhaps even including blocky polyhedral olivines (Welsch et al., 2013) and the entrapment of melt inclusions. After initial inclusion entrapment, continued stirring of the primitive melt and the original magma in the reservoir mixed the melts. These fluid and crystal motions placed the olivines into cooler melts, with a lower Mg# than the melt from which the olivines grew (as shown in **figure 3**).

Owing to the larger thermal contraction of the melt compared to the host olivine, the internal pressure in the melt inclusion decreases during cooling; thus, even for initially vapor-undersaturated melts, eventually the internal pressure will equal the vapor pressure and the melt will become vapor-saturated (Lowenstern, 1995). Meanwhile, PEC of olivine on the inclusion walls will result in increased concentration of both CO_2 and H_2O in the melt. The decrease in internal pressure, combined with increase in CO_2-H_2O concentrations in the melt, will cause nucleation and growth of a vapor bubble. CO_2 (and H_2O) will exsolve to the vapor phase both because of decreasing pressure, and also because their concentrations in the melt increase as a result of PEC. Minor H_2O partitioning into the bubbles did not reduce melt phase H_2O

nucleation and growth of a vapor bubble. CO_2 (and H_2O) will exsolve to the vapor phase both because of decreasing pressure, and also because their concentrations in the melt increase as a result of PEC. Minor H_2O partitioning into the bubbles did not reduce melt phase H_2O concentrations significantly (Steele-Macinnis et al., 2011). **Figure 6a** shows a model for PEC-induced sequestration of CO_2 into a vapor bubble at two pressures, superimposed on the data plot and using the same color scheme, using the published equations for thermal contraction and molar volume differentials (Steele-Macinnis et al., 2011) modified for olivine and basaltic melt. Up to 85% of the CO_2 in the melt inclusion may be sequestered into the bubble when the degree of post-entrapment crystallization reaches 30 mol%. The increase in H_2O concentrations caused by PEC has been corrected for, as for all the other incompatible and compatible elements (see **supplementary material** for a full description of the PEC correction procedure). The melt inclusion data span a range that is consistent with these models. The cooler the carrier magma in the reservoir, the greater the extent of post-entrapment crystallization prior to quenching and eruption, and the more significant the loss of CO_2 from the silicate melt of the inclusion into the bubble. Therefore, the transfer of olivine that grew rapidly from primitive melts into cooler surrounding magma led to the negative correlation between the CO_2 concentration in the silicate part of the melt inclusion, which is what is measured by SIMS analysis and the extent of post-entrapment crystallization.

The link between the measured CO_2 content of the melt inclusions and fountain height can be understood using a similar logic, but in this case we consider the generation of CO_2 bubbles in the open magma reservoir rather than in inclusions. The juxtaposition of hot, possibly CO_2-supersaturated (although our data does not constrain this) primitive melt, carrying an already large load of exsolved CO_2-rich vapour (perhaps >0.5 wt%; Sides et al., 2014), against coolar degassed melt, will lead to olivine crystallization, which will cause exsolution of volatiles through second boiling (**figure 9**). Heating of the cooler stored melts will also induce vesiculation owing to the lowering of solubility with temperature for both H_2O and CO_2. Juxtaposition of hot primitive melt against cool reservoir melts allows for the CO_2 arriving with the hot melt to be harvested into vapour bubbles, potentially increasing overpressure in the chamber and driving higher fountains. This effect may therefore account for the observed negative correlation between melt inclusion CO_2 content and fountain height.

Our work shows that magma mixing is a plausible explanation for the trends in volatile concentrations observed in the products of the 1959 Kīlauea Iki eruption and that the mixing process, driven by drained-back magma that acted as a coolant, was enough to exert an influence on eruption dynamics. Magma mixing and associated vesiculation might have triggered and sustained fountains throughout the latter part of the eruption, when magma intrusion from depth was minimal and the magma budget was dominated by drain-back. How important this mixing and eruption triggering process is in general at Kīlauea and elsewhere is yet to be seen, but one might imagine magma mixing and the associated thermal effects to be important when hot primitive magmas are injected into the rift zones, encountering cooler stored magmas, for example. This study, while cautioning against accepting melt inclusion CO_2 concentrations "as measured" in mixed magmas, also illustrates that careful analysis and interpretation of post-entrapment modifications can turn this apparent challenge into a way to yield new and useful insights.

5. Conclusions

Geochemical data from the Kīlauea Iki melt inclusions, when combined with the magma budget and with contemporaneous observations, show a complex pre-eruptive history involving mixing between hot, geochemically heterogeneous melts from depth, likely carrying exsolved vapour, with stored melts resident in the magma reservoir, and with melts which had erupted at the surface, degassed and drained-back into the reservoir. The drained-back melts acted as a coolant, inducing rapid cooling of the more primitive melts and their olivines prior to eruption and inducing crystallization and vesiculation that may have increased the overpressures in the reservoir enough to trigger fountaining. Concentrations of H_2O and CO_2 in the melt inclusions were sensitive to different aspects of the mixing process. The drained-back lavas were extensively outgassed and there were large contrasts between their H_2O content and that of the stored and intruding magmas; hence mixing between all three components in roughly equal proportions yielded a clear mixing trend. A consequence of this mixing is that the melts became

extensively outgassed and there were large contrasts between their H_2O content and that of the stored and intruding magmas; hence mixing between all three components in roughly equal proportions yielded a clear mixing trend. A consequence of this mixing is that the melts became vapor-undersaturated, meaning that equilibration pressures cannot be inferred from their volatile composition using saturation models. CO_2, in contrast, would have recorded a much weaker mixing signature because the shallow stored melts would have had only a few hundred ppm CO_2 and the drained-back lavas < 50 ppm (contrast this to the case for H_2O, where stored melts contained > 0.6 wt% H_2O and drained-back melts <0.1 wt%). So, even without a post-entrapment modification, the mixing trend recorded by the CO_2 concentrations would have been much weaker. After the melt inclusions were trapped, the continued growth of a vapor bubble, caused by enhanced post-entrapment crystallization, sequestered a large fraction of CO_2 from the melt, resulting in the mixing signature being completely overprinted. This overprinting did not occur for H_2O because, when the melt becomes entirely H_2O dominated, exsolution of H_2O will tend to increase the internal pressure, not decrease it as in the case for CO_2, owing to the difference in partial molar volumes of dissolved versus vapor-phase H_2O. We do not, however, rule out other processes such as diffusive loss of H+ and gas flushing as important in the system. A negative correlation between the CO_2 concentration in the melt inclusion and fountain height further suggests that this mixing and cooling process was a primary control on eruption dynamics through the rapid vesiculation mechanism. As well as delivering important new insights into the links between melt geochemistry, volatile behaviour and volcanology at Kīlauea, we suggest that this work also cautions against accepting the volatile concentrations of melt inclusions as representative of pre-entrapment melts, in accordance with the growing body of other work in this area.

Acknowledgements

IS was supported by a NERC-funded studentship and a USGS Jack Kleinman Grant for Volcano Research. ME acknowledges NERC ion probe grant IMF376/0509. BH's participation was funded by NSF EAR-1145159. We acknowledge the NERC Edinburgh Ion Microprobe facility, where we undertook the SIMS analyses. Richard Hinton, Cees-Jan De Hoog, John Craven, Chiara Petrone, Jason Day, and Martin Walker for assistance with data collection. We thank 3 anonymous reviewers for improving the manuscript considerably.

References

Anderson, A.T., Brown, G.G., 1993. CO2 contents and formation pressures of some Kilauean melt inclusions. American Mineralogist 78, 794-803.

Baker, D., 2008. The fidelity of melt inclusions as records of melt composition. Contr. Mineral. and Petrol. 156, 377-395.

Bottinga, Y., Javoy, M., 1991. The degassing of Hawaiian tholeiite. Bull Volcanol 53, 73-85.

Clague, D.A., Weber, W.S., Dixon, J.E., 1991. Picritic glasses from Hawaii. Nature 353, 553-556.

Danyushevsky, L.V., Plechov, P., 2011. Petrolog3: Integrated software for modeling crystallization processes. Geochemistry, Geophysics, Geosystems 12, Q07021.

Davidson, J.P., Morgan, D.J., Charlier, B.L.A., Harlou, R., Hora, J.M., 2007. Microsampling and Isotopic Analysis of Igneous Rocks: Implications for the Study of Magmatic Systems. Annual Review of Earth and Planetary Sciences 35, 273-311.

Demouchy, S., Mackwell, S., 2003. Water diffusion in synthetic iron-free forsterite. Physics and Chemistry of Minerals 30, 486-494.

Dixon, J.E., 1997. Degassing of alkalic basalts. American Mineralogist 82, 368-378.

Dixon, J.E., Clague, D.A., Stolper, E.M., 1991. Degassing history of water, sulfur, and carbon in submarine lavas from Kīlauea Volcano, Hawaii. The Journal of Geology, 371-394.

Eaton, J., Richter, D., Krivoy, H., 1987. Cycling of magma between the summit reservoir and Kīlauea Iki lava lake during the 1959 eruption of Kīlauea volcano. US Geol. Surv. Prof. Pap 1350, 1307-1335.

Edmonds, M., Gerlach, T.M., Herd, R.A., 2009. Halogen degassing during ascent and eruption of water-poor basaltic magma. Chemical Geology 263, 122-130.

Edmonds, M., Sides, I.R., Maclennan, J., 2014. Insights into mixing, fractionation and degassing of primitive melts at Kīlauea Volcano, Hawai`i. AGU Monograph.

Fagents, S.A., Wilson, L., 1995. Explosive volcanism on Venus: Transient volcanic explosions as a mechanism for localized pyroclast dispersal. Journal of Geophysical Research: Planets 100, 26327-26338.

Fiske, R.S., Kinoshita, W.T., 1969. Inflation of Kīlauea volcano prior to its 1967-1968 eruption. Science (New York, NY) 165, 341

mechanism for localized pyroclast dispersal. Journal of Geophysical Research: Planets 100, 26327-26338.
Fiske, R.S., Kinoshita, W.T., 1969. Inflation of Kīlauea volcano prior to its 1967-1968 eruption. Science (New York, NY) 165, 341.
Gaetani, G.A., O'Leary, J.A., Shimizu, N., Bucholz, C.E., Newville, M., 2012. Rapid reequilibration of H2O and oxygen fugacity in olivine-hosted melt inclusions. Geology 40, 915-918.
Garcia, M.O., Pietruszka, A.J., Rhodes, J.M., 2003. A Petrologic Perspective of Kīlauea Volcano's Summit Magma Reservoir. Journal of Petrology 44, 2313-2339.
Gerlach, T.M., 1986. Exsolution of H2O, CO2, and S during eruptive episodes at Kīlauea Volcano, Hawaii. Journal of Geophysical Research: Solid Earth 91, 12177-12185.
Gerlach, T.M., Graeber, E.J., 1985. Volatile budget of Kīlauea volcano. Nature 313, 273-277.
Gerlach, T.M., McGee, K.A., Elias, T., Sutton, A.J., Doukas, M.P., 2002. Carbon dioxide emission rate of Kīlauea Volcano: Implications for primary magma and the summit reservoir. Journal of Geophysical Research: Solid Earth 107, 2189.
Hauri, E., 2002. SIMS analysis of volatiles in silicate glasses, 2: isotopes and abundances in Hawaiian melt inclusions. Chemical Geology 183, 115-141.
Head, J.W., Wilson, L., 1987. Lava fountain heights at Pu'u 'O'o, Kīlauea, Hawaii: Indicators of amount and variations of exsolved magma volatiles. Journal of Geophysical Research: Solid Earth 92, 13715-13719.
Houghton, B.F., Gonnermann, H.M., 2008. Basaltic explosive volcanism: Constraints from deposits and models. Chemie der Erde - Geochemistry 68, 117-140.
James, M.R., Lane, S.J., Houghton, B.A., 2013. "Unsteady" explosive eruptions: Strombolian activity.
Jaupart, C., Vergniolle, S., 1988. Laboratory models of Hawaiian and Strombolian eruptions. Nature 331, 58-60.
Johnson, E.R., Wallace, P.J., Cashman, K.V., Granados, H.D., Kent, A.J., 2008. Magmatic volatile contents and degassing-induced crystallization at Volcán Jorullo, Mexico: implications for melt evolution and the plumbing systems of monogenetic volcanoes. Earth and Planetary Science Letters 269, 478-487.
Jurewicz, A.G., Watson, E.B., 1988. Cations in olivine, Part 2: Diffusion in olivine xenocrysts, with applications to petrology and mineral physics. Contr. Mineral. and Petrol. 99, 186-201.
Kent, A.J., Elliott, T.R., 2002. Melt inclusions from Marianas arc lavas: implications for the composition and formation of island arc magmas. Chemical Geology 183, 263-286.
Kent, A.J.R., 2008. Melt Inclusions in Basaltic and Related Volcanic Rocks. Reviews in Mineralogy and Geochemistry 69, 273-331.
Klawonn, M., Houghton, B.F., Swanson, D.A., Fagents, S.A., Wessel, P., Wolfe, C.J., 2014. Constraining explosive volcanism: subjective choices during estimates of eruption magnitude. Bull Volcanol 76, 1-6.
Lloyd, A.S., Plank, T., Ruprecht, P., Hauri, E.H., Rose, W., 2013. Volatile loss from melt inclusions in pyroclasts of differing sizes. Contr. Mineral. and Petrol. 165, 129-153.
Lowenstern, J.B., 1995. Applications of silicate-melt inclusions to the study of magmatic volatiles. Magmas, fluids, and ore deposits 23, 71-99.
Maclennan, J., 2008. Concurrent Mixing and Cooling of Melts under Iceland. Journal of Petrology 49, 1931-1953.
Marske, J., Garcia, M., Pietruszka, A., Rhodes, J., Norman, M., Heaton, D., 2010. Evolution of Kilauea Volcano's shallow magmatic plumbing system: a geochemical perspective from historical rift lavas (1790-present), AGU Fall Meeting Abstracts, p. 2346.
Mather, T.A., Witt, M.L.I., Pyle, D.M., Quayle, B.M., Aiuppa, A., Bagnato, E., Martin, R.S., Sims, K.W.W., Edmonds, M., Sutton, A.J., Ilyinskaya, E., 2012. Halogens and trace metal emissions from the ongoing 2008 summit eruption of Kīlauea volcano, Hawai`i. Geochimica et Cosmochimica Acta 83, 292-323.
Métrich, N., Wallace, P.J., 2008. Volatile Abundances in Basaltic Magmas and Their Degassing Paths Tracked by Melt Inclusions. Reviews in Mineralogy and Geochemistry 69, 363-402.
Moore, G., Vennemann, T., Carmichael, I., 1998. An empirical model for the solubility of H2O in magmas to 3 kilobars. American Mineralogist 83, 36-42.
Murata, K.J., Richter, D.H., 1966. The settling of olivine in Kilauean magma as shown by lavas of the 1959 eruption. American Journal of Science 264, 194-203.
Newman, S., Lowenstern, J.B., 2002. VolatileCalc: a silicate melt–H2O–CO2 solution model written in Visual Basic for excel. Computers & Geosciences 28, 597-604.
Parfitt, E.A., 2004. A discussion of the mechanisms of explosive basaltic eruptions. Journal of Volcanology and Geothermal Research 134, 77-107.
Parfitt, E.A., Wilson, L., Neal, C.A., 1995. Factors influencing the height of Hawaiian lava fountains: implications for the use of fountain height as an indicator of magma gas content. Bull Volcanol 57, 440-450.
Pietruszka, A.J., Garcia, M.O., 1999a. A Rapid Fluctuation in the Mantle Source and Melting History of Kīlauea Volcano Inferred from the Geochemistry of its Historical Summit Lavas (1790–1982). Journal of Petrology 40, 1321-1342.
Pietruszka, A.J., Garcia, M.O., 1999b. The size and shape of Kīlauea Volcano's summit magma storage reservoir: a geochemical probe. Earth and Planetary Science Letters 167, 311-320.
Pietruszka, A.J., Norman, M.D., Garcia, M.O., Marske, J.P., Burns, D.H., 2012. Chemical heterogeneity in the Hawaiian mantle plume from the alteration and dehydration of recycled oceanic crust. Earth and Planetary Science Letters

reservoir: a geochemical probe. Earth and Planetary Science Letters 107, 511-526.
Pietruszka, A.J., Norman, M.D., Garcia, M.O., Marske, J.P., Burns, D.H., 2012. Chemical heterogeneity in the Hawaiian mantle plume from the alteration and dehydration of recycled oceanic crust. Earth and Planetary Science Letters.
Portnyagin, M., Almeev, R., Matveev, S., Holtz, F., 2008. Experimental evidence for rapid water exchange between melt inclusions in olivine and host magma. Earth and Planetary Science Letters 272, 541-552.
Qin, Z., Lu, F., Anderson, A.T., 1992. Diffuse reequilibration of melt and fluid inclusions. The American mineralogist 77, 565-576.
Roeder, P.L., Emslie, R.F., 1970. Olivine-liquid equilibrium. Contr. Mineral. and Petrol. 29, 275-289.
Ryan, M.P., Koyanagi, R.Y., Fiske, R.S., 1981. Modeling the three−dimensional structure of macroscopic magma transport systems: Application to Kilauea Volcano, Hawaii. Journal of Geophysical Research: Solid Earth (1978–2012) 86, 7111-7129.
Sides, I.R., Edmonds, M., Maclennan, J., Swanson, D.A., Houghton, B.F., 2014. Eruption style at Kīlauea Volcano in Hawai`i linked to primary melt composition Nature Geoscience.
Sigvaldason, G.E., Óskarsson, N., 1976. Chlorine in basalts from Iceland. Geochimica et Cosmochimica Acta 40, 777-789.
Slezin, Y.B., 2003. The mechanism of volcanic eruptions (a steady state approach). Journal of Volcanology and Geothermal Research 122, 7-50.
Sobolev, A., 1996. Melt inclusions in minerals as a source of principle petrological information. Petrology 4, 209-220.
Spilliaert, N., Allard, P., Métrich, N., Sobolev, A., 2006. Melt inclusion record of the conditions of ascent, degassing, and extrusion of volatile−rich alkali basalt during the powerful 2002 flank eruption of Mount Etna (Italy). Journal of Geophysical Research: Solid Earth (1978–2012) 111.
Steele-Macinnis, M., Esposito, R., Bodnar, R.J., 2011. Thermodynamic model for the effect of post-entrapment crystallization on the H2O–CO2 systematics of vapor-saturated, silicate melt inclusions. Journal of Petrology 52, 2461-2482.
Stovall, W., Houghton, B., Hammer, J., Fagents, S., Swanson, D., 2012. Vesiculation of high fountaining Hawaiian eruptions: episodes 15 and 16 of 1959 Kīlauea Iki. Bull Volcanol 74, 441-455.
Stovall, W., Houghton, B.F., Gonnermann, H., Fagents, S.A., Swanson, D.A., 2011. Eruption dynamics of Hawaiian-style fountains: the case study of episode 1 of the Kīlauea Iki 1959 eruption. Bull Volcanol 73, 511-529.
Vergniolle, S., 1996. Bubble size distribution in magma chambers and dynamics of basaltic eruptions. Earth and Planetary Science Letters 140, 269-279.
Vergniolle, S., 2008. From sound waves to bubbling within a magma reservoir: comparison between eruptions at Etna (2001, Italy) and Kīlauea (Hawaii). Geological Society, London, Special Publications 307, 125-146.
Vergniolle, S., Jaupart, C., 1986. Separated two-phase flow and basaltic eruptions. Journal of Geophysical Research: Solid Earth 91, 12842-12860.
Wallace, P., Carmichael, I.S.E., 1992. Sulfur in basaltic magmas. Geochimica et Cosmochimica Acta 56, 1863-1874.
Wallace, P.J., Anderson, A.T., 1998. Effects of eruption and lava drainback on the H2O contents of basaltic magmas at Kīlauea Volcano. Bull Volcanol 59, 327-344.
Welsch, B., Faure, F., Famin, V., Baronnet, A., Bachèlery, P., 2013. Dendritic Crystallization: A Single Process for all the Textures of Olivine in Basalts? Journal of Petrology 54, 539-574.
Wilson, L., Head, J.W., 1988. "Nature of local magma storage zones and geometry of conduit systems below basaltic eruption sites: Pu'u 'O 'o, Kīlauea East Rift, Hawaii, Example"". Journal of Geophysical Research: Solid Earth 93, 14785-14792.
Wright, T.L., 1973. Magma Mixing as Illustrated by the 1959 Eruption, Kīlauea Volcano, Hawaii. Geological Society of America Bulletin 84, 849-858.

Figure captions

Figure 1: Maps showing the location of Kīlauea Iki and the sampling sites at Kīlauea Volcano, Hawai`i: a) the location of Kīlauea Iki crater; b) tephra deposit produced by the Kīlauea Iki eruption and the location of sampling pits utilized in this study.

Figure 2: The magma budget of the 1959 Kīlauea Iki eruption, Hawai`i from Eaton et al. (1987), deduced from contemporaneous tilt measurements, calibrated by detailed observations of lava lake level (Richter et al., 1970).

Figure 3: The relationship between olivines and their carrier liquids. Olivine core composition (forsterite %) compared with averaged matrix glass Mg number for each eruptive episode (with the Fe^{2+} set to 90% of total Fe) produced during the Kīlauea Iki 1959 eruption. The solid black line is the equilibrium olivine composition for a given Mg# at K_D=0.3. The dotted black lines are calculated equilibrium compositions at K_D=0.27 and 0.33.

Figure 4: Major, minor and trace element geochemistry of the melt inclusions and matrix glasses

calculated equilibrium compositions at K_D=0.27 and 0.33.

Figure 4: Major, minor and trace element geochemistry of the melt inclusions and matrix glasses of the 1959 Kīlauea Iki (colour-coded for episode number) and 1960 Kapoho eruptions plotted against MgO content on the x axis: a) Al_2O_3 (wt%); b) TiO_2 (wt%); c) CaO/Al_2O_3; d) La (ppm); e) Ba (ppm) and f) Sc (ppm). All element oxide abundances have been corrected for post-entrapment crystallization as described in the **supplementary material**.

Figure 5: (a) La versus Yb (units of ppm). Lines of constant La/Yb ratio are marked; (b) the standard deviation of the population of Nb/Y ratios in melt inclusions erupted from each episode, plotted against the "inflation volume" which is the volume of magma inferred to have intruded the summit reservoir prior to each episode, deduced from tilt measurements (Eaton et al., 1987). The 95% confidence interval for each estimate of the standard deviation, based on sample size, is shown as a vertical bar.

Figure 6: Volatile systematics of the melt inclusions: a) H_2O against CO_2 concentrations for the melt inclusions of the 1959–60 eruptions of Kīlauea Iki and Kapoho. The data are color-coded for the degree of post-entrapment crystallization the melt inclusions experienced, deduced from the disequilibrium between melt and adjacent olivine (Danyushevsky and Plechov, 2011). Also marked are horizontal lines representing the outcomes of a model to describe the sequestration of CO_2 into a vapor bubble during post-entrapment crystallization (Steele-Macinnis et al., 2011), color-coded in the same way as the data; b) H_2O against CO_2 concentrations for the melt inclusions of the 1959–60 eruptions of Kīlauea Iki and Kapoho. The data are color-coded for episode number (shown in legend). Isobars are shown in grey, and were calculated using VolatileCalc (Newman and Lowenstern, 2002); c) H_2O versus S concentrations; and d) H_2O versus Cl concentrations, both color-coded for episode number.

Figure 7: The link between melt inclusion composition and eruption dynamics: a) the H_2O-CO_2 plot color-coded for fountain height and b) mean (grey) and maximum (black) CO_2 concentrations in the melt inclusions erupted during each episode plotted against the maximum fountain height for each episode (in metres).

Figure 8: Application of the magma mixing model of Wallace and Anderson (1998) to the melt inclusion data. The concentrations of (a) H_2O and (b) CO_2 in the melt inclusions (black solid circles) plotted against episode number. The mean concentrations for each episode are grey circles. Also shown are the predictions for volatile concentrations based on the mixing model (dashed lines; described in supplementary material). Fountain heights were measured by theodolite (Richter et al., 1970) and the precision of the measurements is better than 1 m (the theodolite is precise to 2-3 seconds of an arc, and the measurements were made at a range of 1 km). We use the maximum height of the opaque "core" of the fountain, not the maximum height achieved by individual clasts. This measurement inevitably comes with an element of subjectivity, leading to a relative error that we judge to be not more than 1-2 metres.

Figure 9: Schematic diagram to show the processes of magma mixing and vesiculation during the 1959 Kīlauea Iki eruption. Intrusion of hot, gas-rich picritic melt, which contains highly forsteritic olivines, takes place into the summit magma reservoir, which contains relatively cooler, stored melts, with less forsteritic olivines, which have lost their gases due to buoyant bubble rise and escape at the top of the reservoir. Turbulent mixing is a consequence of the high Reynolds number of the intruding magma. The picritic melt crystallizes on contact with the cooler melt, and, once the eruptions had started, the much cooler drained-back lavas, inducing further rapid vesiculation. Cooling of the hot primitive melts against the cool drained-back lavas causes existing olivines to grow rapidly, trapping melt as inclusions. Olivines in the drained-back and stored melts near to the contact with the hot picrite may undergo partial resorption. Melt inclusions may develop vapor bubbles if they cool after entrapment. Some inclusions may be associated with a "pre-entrapment" bubble, representing a bubble that was trapped, along with the melt, during rapid crystallization. The mixed magma erupts as a fountain. The degassed, cool magma is drained-back down the conduit and mixed into the reservoir, enhancing the cooling of primitive melts at depth. The magma is further mixed, such that olivines that were originally associated with the stored and drained-back melts, and olivines that were originally associated with the intruding melt, are distributed. The mixed magma is gas-rich. Further cooling of the olivines in the mixed magma causes post-entrapment crystallization (thick green rim inside the melt inclusions), which acts to increase the size and mass of the vapor bubble by inducing a

with the intruding melt, are distributed. The mixed magma is gas-rich. Further cooling of the olivines in the mixed magma causes post-entrapment crystallization (thick green rim inside the melt inclusions), which acts to increase the size and mass of the vapor bubble by inducing a pressure drop inside the inclusion. The bubbles may sequester up to 85 wt% of the total CO_2 inside the inclusion.

Eruption episode	*Duration (hours)* [a]	*Repose time after episode (hours)* [a]	*Maximum fountain height (m)* [a]	*Eruption rate (m^3/s)* [a]	*Relative volume reservoir (10^6 m^3)* [b]	*Deflation volume (10^6 m^3)* [c]	*Inflation volume (10^6 m^3)* [c]	*Erupted volume (10^6 m^3)* [d]	*Drain back volume (10^6 m^3)* [d]
1	167	101	380	83	30.6	-	-	30.6	1.1
2	15	48	305	102	10.4	2.8	13.1	3.6	4.5
3	29	101	520	53	22.0	8.6	2.8	3.2	2.0
4	32	26	200	130	30.6	6.3	6.3	11.5	6.3
5	9	15	380	324	33.6	6.0	4.7	6.5	4.7
6	11	11	245	215	33.6	5.7	4.6	6.6	3.8
7	7	42	425	198	36.1	4.4	2.1	3.7	5.6
8	19	17	335	124	40.4	6.2	3.7	6.7	6.0
9	8	14	213	278	38.5	5.7	4.0	5.7	6.9
10	8	9	335	313	41.0	5.0	6.0	6.3	4.9
11	4	16	365	417	39.8	5.2	4.1	4.7	4.1
12	2	604	335	417	42.8	2.1	4.7	2.2	3.1
13	4	9	350	313	42.8	3.9	1.8	3.2	2.4
14	2	8	350	417	41.6	1.8	1.0	1.8	1.0
15	4	35	580	243	38.5	1.9	0.7	1.7	3.2
16	3	-	455	556	39.1	3.9	3.4	4.1	4.1

Table 1: Summary of the physical properties and magma budget of the 1959 Kilauea Iki eruption.

a from direct observations by Macdonald (1962) and Richter (1970).

b the summit reservoir volume at the start of each episode, relative to the reservoir volume at the end of episode 1 (from Eaton et al., 1987).

c Volumes of lava inferred to have caused the inflation prior to each episode and the deflation syn- and post-episode (from Eaton et al (1987).

d volumes of lava erupted and drained back from observations of the lava lake level at the surface (from Richter, 1970).

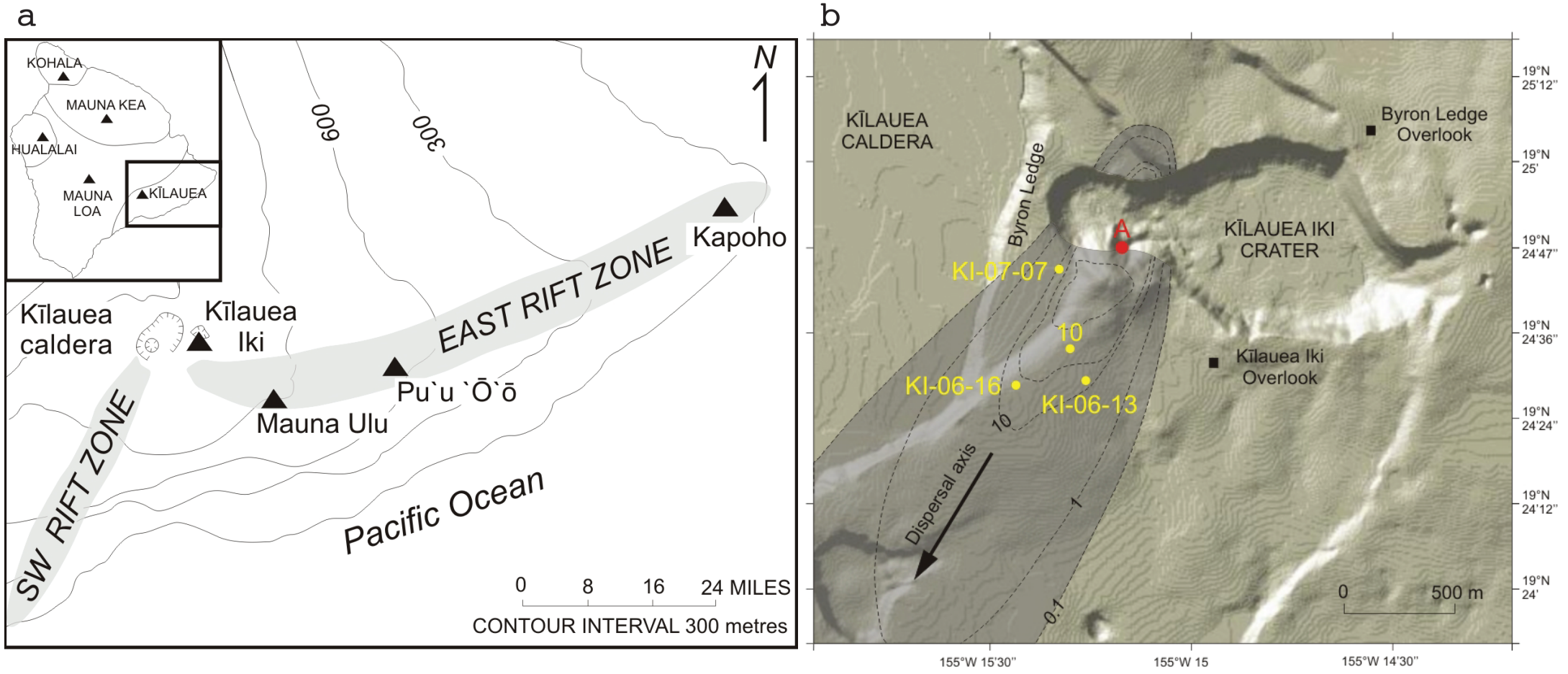
a
KOHALA
MAUNA KEA
HUALALAI
MAUNA LOA
KĪLAUEA
N
600
300
Kīlauea caldera
Kīlauea Iki
EAST RIFT ZONE
Kapoho
Pu`u `Ō`ō
Mauna Ulu
SW RIFT ZONE
Pacific Ocean
0 8 16 24 MILES
CONTOUR INTERVAL 300 metres
b
KĪLAUEA CALDERA
Byron Ledge
Byron Ledge Overlook
KĪLAUEA IKI CRATER
A
KI-07-07
10
KI-06-16
KI-06-13
Kīlauea Iki Overlook
10
1
0.1
Dispersal axis
0 500 m
19°N 25'12"
19°N 25'
19°N 24'47"
19°N 24'36"
19°N 24'24"
19°N 24'12"
19°N 24'
155°W 15'30"
155°W 15
155°W 14'30"

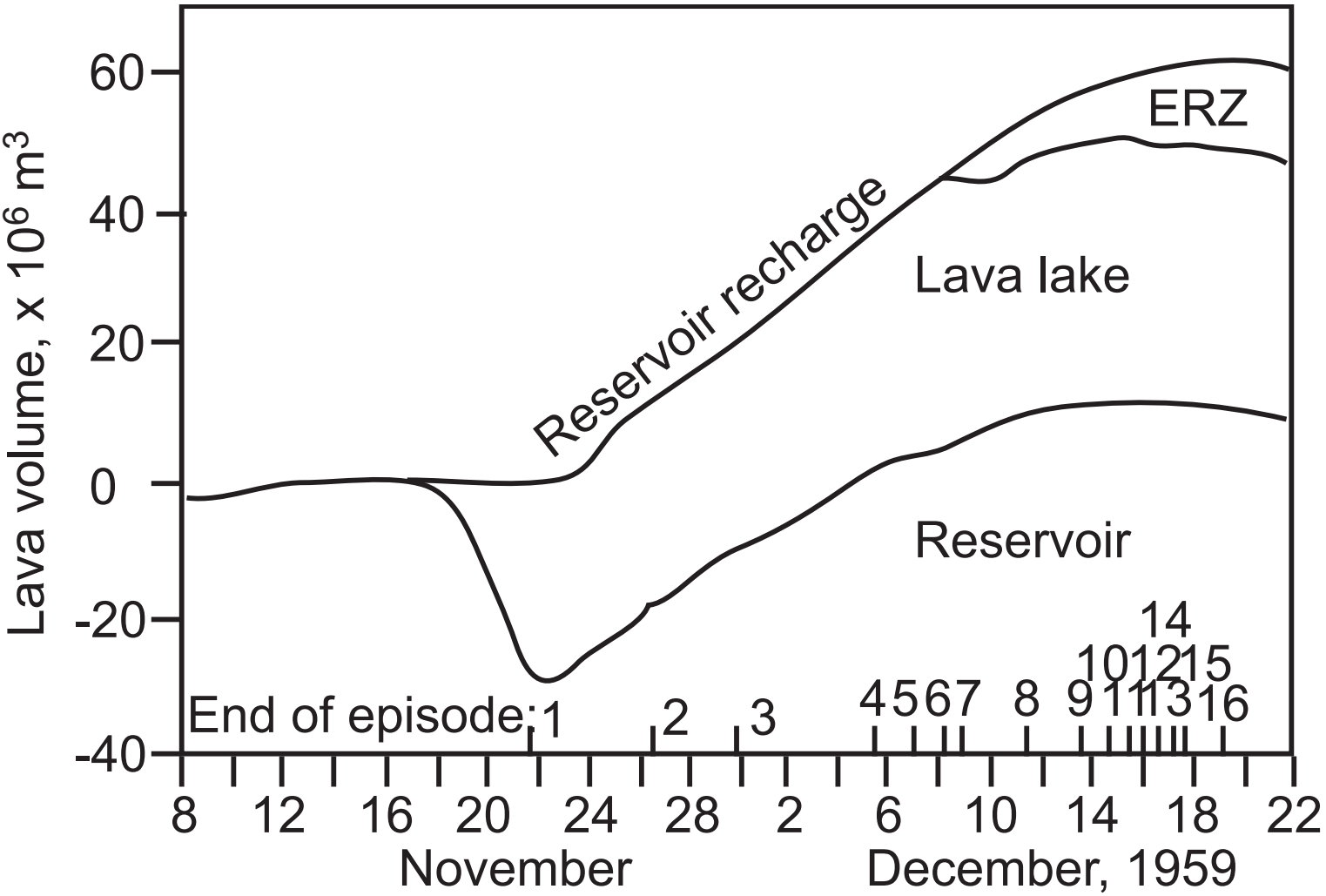
Lava volume, x 10^6 m^3
60
40
20
0
-20
-40
ERZ
Reservoir recharge
Lava lake
Reservoir
End of episode:
1
2
3
4
5
6
7
8
9
10
11
12
13
14
15
16
8
12
16
20
24
28
2
6
10
14
18
22
November
December, 1959

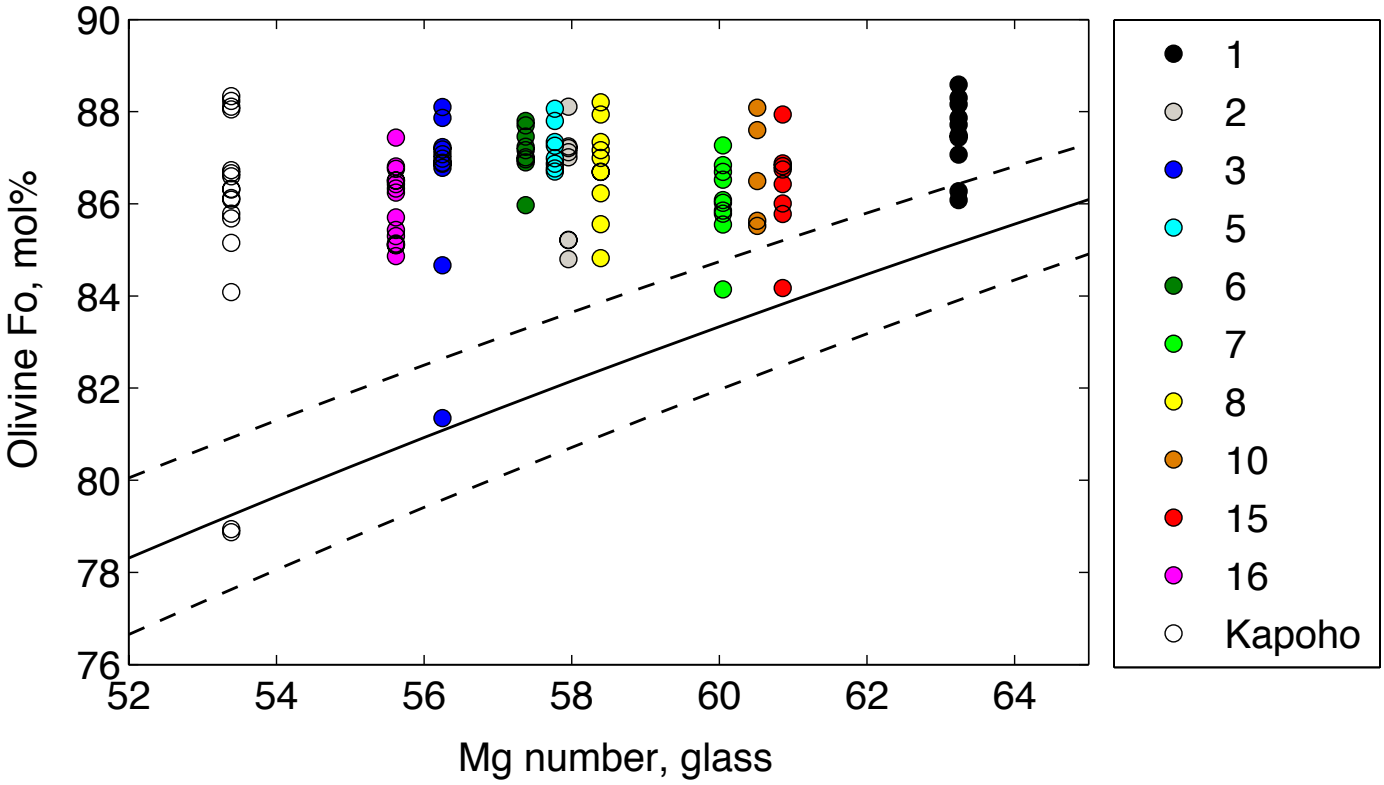
Olivine Fo, mol%
90
88
86
84
82
80
78
76
52
54
56
58
60
62
64
Mg number, glass
1
2
3
5
6
7
8
10
15
16
Kapoho

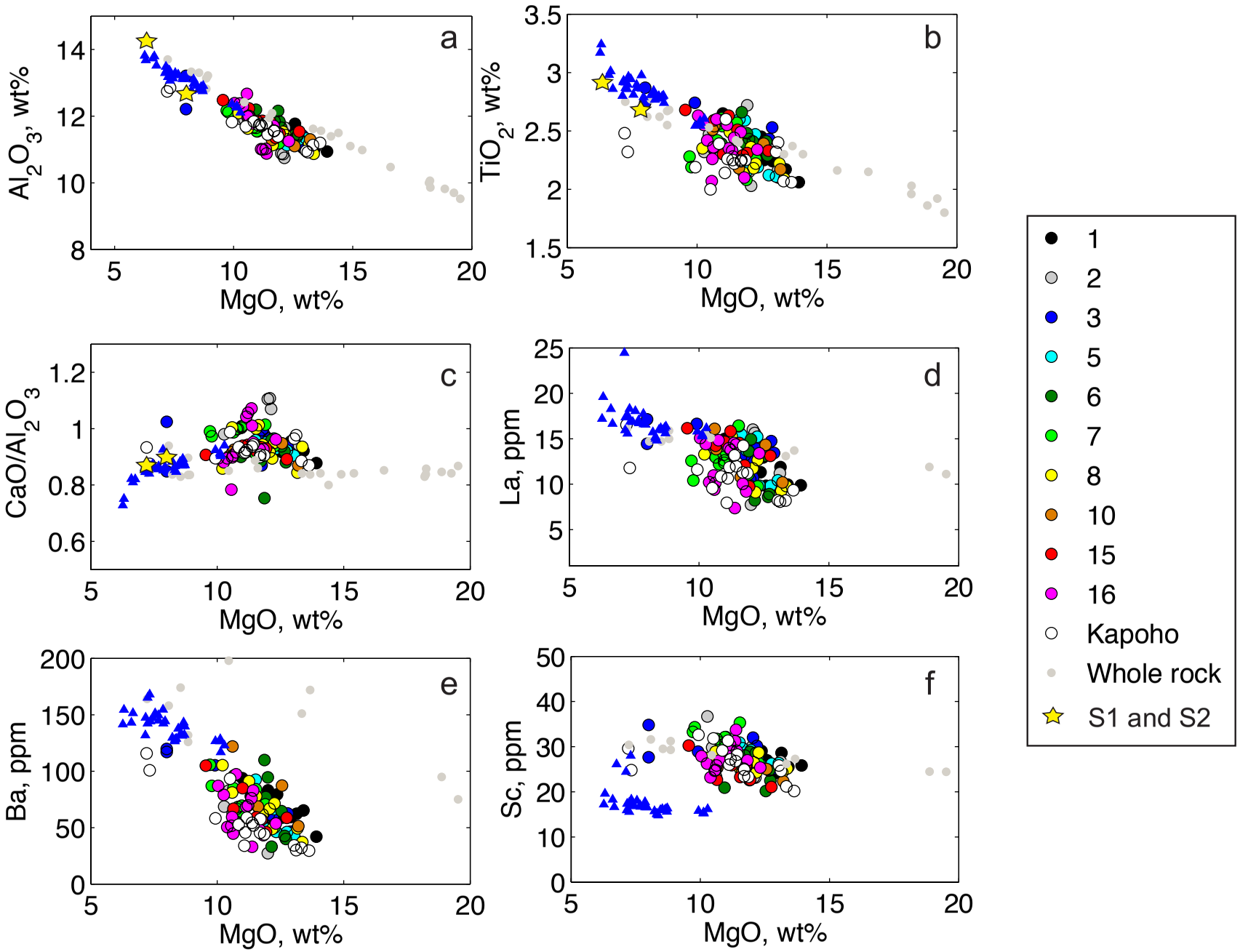
a
b
c
d
e
f
Al_2O_3, wt%
TiO_2, wt%
CaO/Al_2O_3
La, ppm
Ba, ppm
Sc, ppm
MgO, wt%
1
2
3
5
6
7
8
10
15
16
Kapoho
Whole rock
S1 and S2

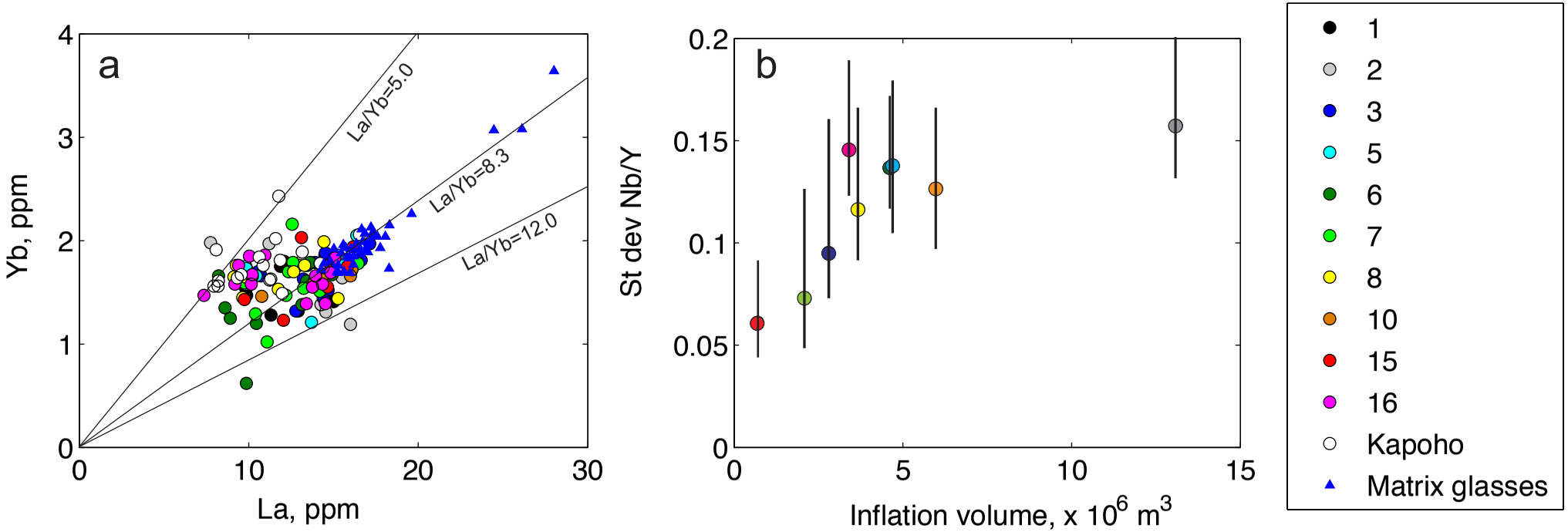
a
b
Yb, ppm
La, ppm
La/Yb=5.0
La/Yb=8.3
La/Yb=12.0
St dev Nb/Y
Inflation volume, x 10^6 m^3
1
2
3
5
6
7
8
10
15
16
Kapoho
Matrix glasses

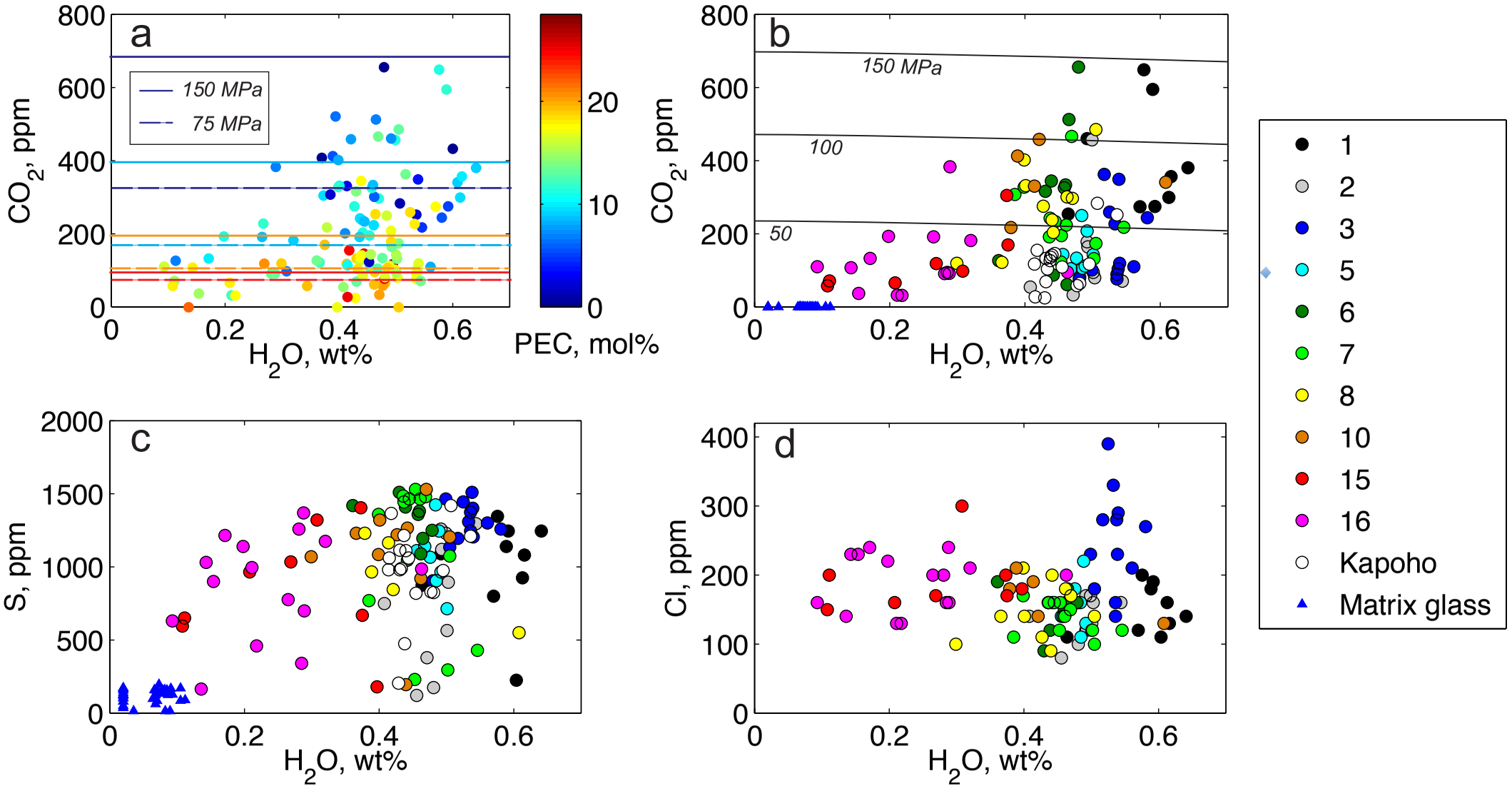
a
150 MPa
75 MPa
CO2, ppm
H2O, wt%
PEC, mol%
b
150 MPa
100
50
c
S, ppm
d
Cl, ppm
1
2
3
5
6
7
8
10
15
16
Kapoho
Matrix glass

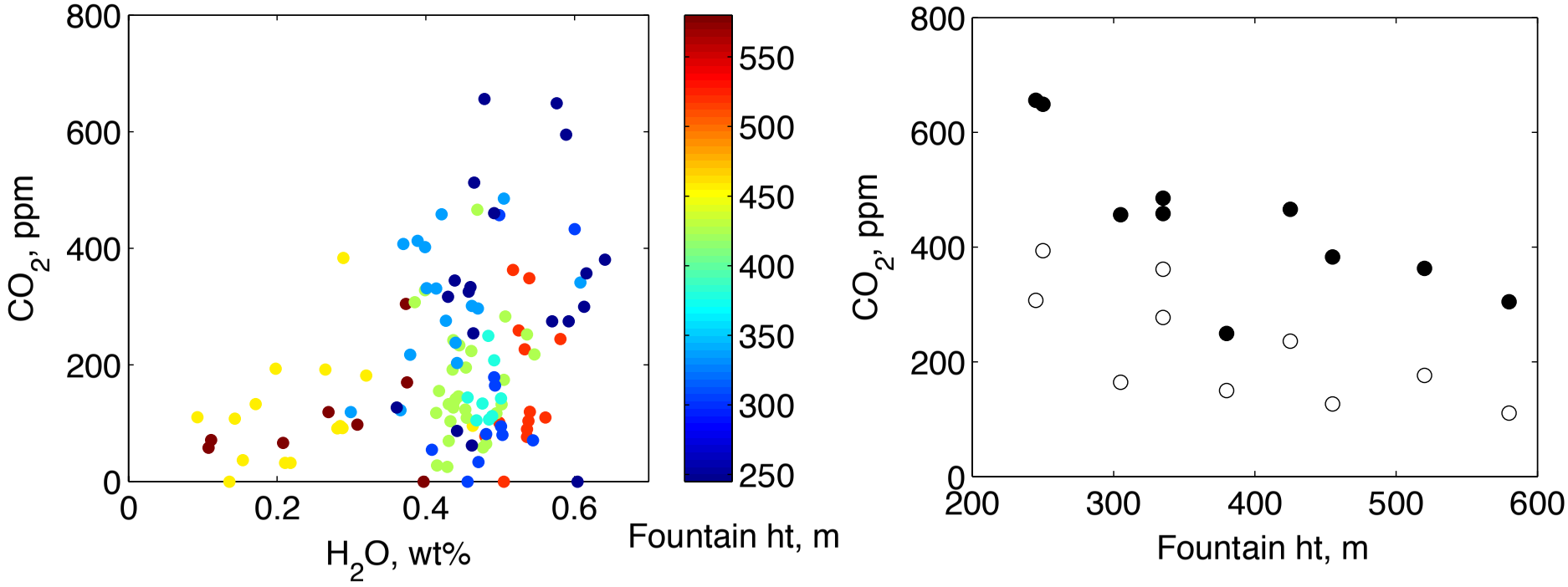
800
600
400
200
0
CO_2, ppm
0
0.2
0.4
0.6
H_2O, wt%
550
500
450
400
350
300
250
Fountain ht, m
800
600
400
200
0
CO_2, ppm
200
300
400
500
600
Fountain ht, m

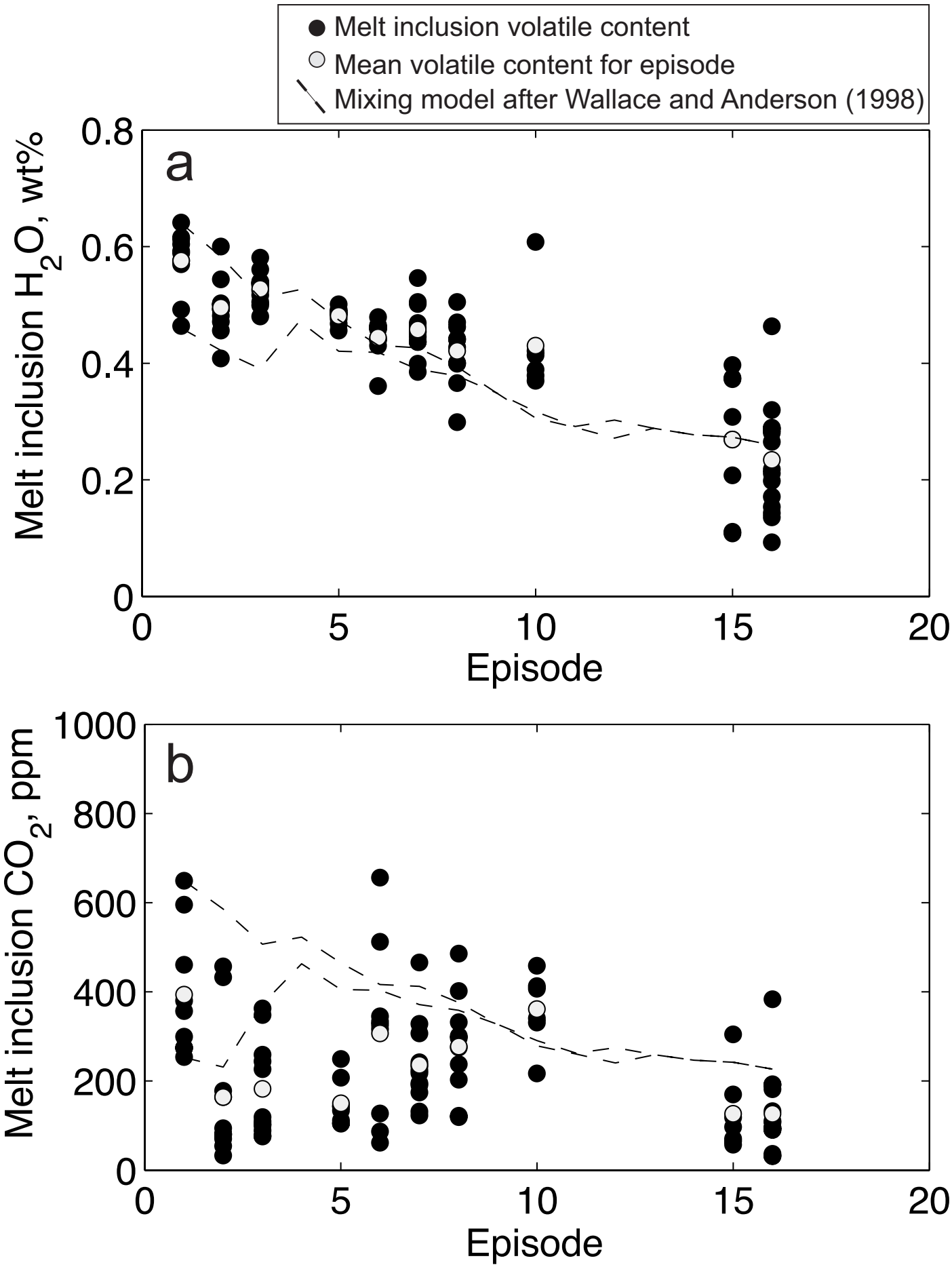
Melt inclusion volatile content
Mean volatile content for episode
Mixing model after Wallace and Anderson (1998)
a
Melt inclusion H_2O, wt%
0.8
0.6
0.4
0.2
0
0
5
10
15
20
Episode
b
Melt inclusion CO_2, ppm
1000
800
600
400
200
0
0
5
10
15
20
Episode

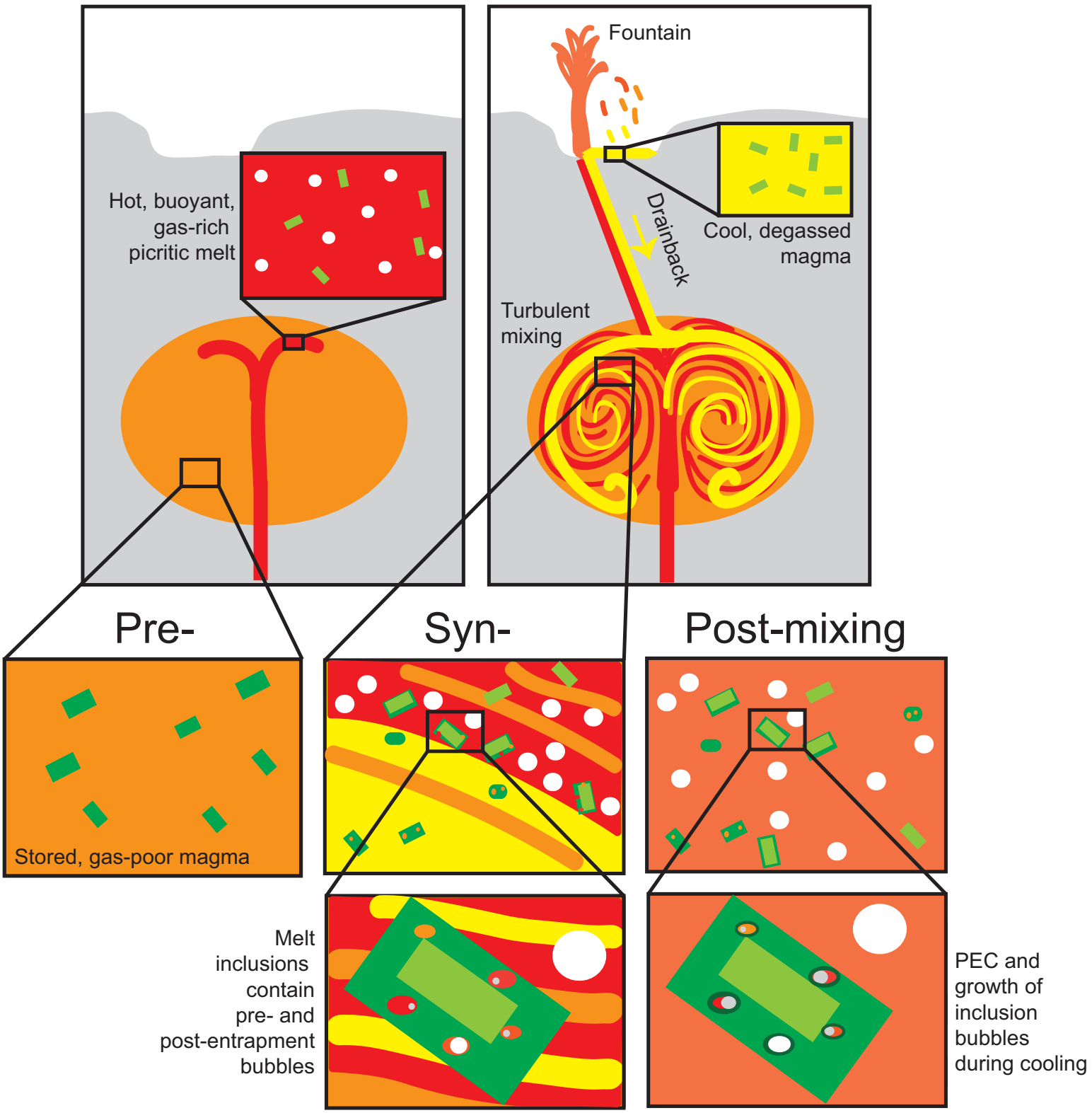
Fountain
Hot, buoyant, gas-rich picritic melt
Drainback
Cool, degassed magma
Turbulent mixing
Pre-
Syn-
Post-mixing
Stored, gas-poor magma
Melt inclusions contain pre- and post-entrapment bubbles
PEC and growth of inclusion bubbles during cooling